Progress In Electromagnetics Research M, Vol. 94, 131–142, 2020

Analysis of Interference between Vast Numbers of Automotive Radars Considering Stochastic Temporal Conditions

Konstantin Hahmann[1, *], Stefan Schneider[1], and Thomas Zwick[2]

Abstract—With a constantly increasing number of cars equipped with 77 GHz automotive radar, the performance degrading effects of crosstalk are becoming a rising threat to radar-enabled automated driving functions. Since interference is sensitive to slight changes of temporal and spatial conditions of the scenario, meaningful measurements are hard to conduct which is why simulations are an important supplement. In this paper, a simulation model is introduced that estimates the distribution of the reduction of the detection range of automotive radars due to multiple interferers focusing on stochastic temporal conditions. The underlying system model calculates the direction- and timing-dependent influence of one single interferer on the detection range of the host radar. The model is kept simple, making it suitable for Monte Carlo methods, which allow the indispensable statistical evaluation of the broadly spread results. Finally, a method is presented that transfers multiple statistics regarding single interferers into a single environment. The computing time of the simulation grows linearly with the number of interfering radars, so the effects of vast numbers of interferers can be studied using this simulation model. Statistical evaluations of the detection performance degradation of a front-mounted radar in sample highway scenarios, containing up to ten interfering radar sensors, are performed in this paper.

1. INTRODUCTION

Frequency modulated continuous wave (FMCW) radars are proven robust and affordable sensors for environment perception. They are widely used in entry-level driver assistance systems as well as in highly advanced automated driving systems [1]. However, the risk of mutual interference grows with rising market penetration. For FMCW radars, two basic principles of mutual interference have been identified:

- Crossing frequency chirps result in an increased noise floor leading to a reduction of the detection range [2, 3].
- Parallel chirps may result in higher false-positive detection rates [4].

Both effects only occur if certain spatial and temporal conditions are met (Fig. 1). The resulting level of interference is highly sensitive to minor changes of these conditions. Regarding the temporal conditions, this is because of narrow bandwidth receivers, low duty cycles, and a large variety of transmission patterns. Since radar systems of different road users are not synchronized in the year 2020, there is a major statistical aspect to interference. Therefore, experiments regarding interference effects are hard to reproduce, and representative results are not guaranteed without comprehensive repetitions of each test. The variety of interference levels grows even further when the experiment includes multiple interferers. Effects of multiple interfering radars on the performance of automotive radars have been covered in [5–9]. These publications focus on the influence of spatial arrangements of the scenario

Received 18 May 2020, Accepted 7 July 2020, Scheduled 16 July 2020
* Corresponding author: Konstantin Hahmann (konstantin.hahmann@daimler.com).
[1] Daimler AG, Germany. [2] Institute of Radio Frequency Engineering and Electronics, Karlsruhe Institute of Technology, Germany.

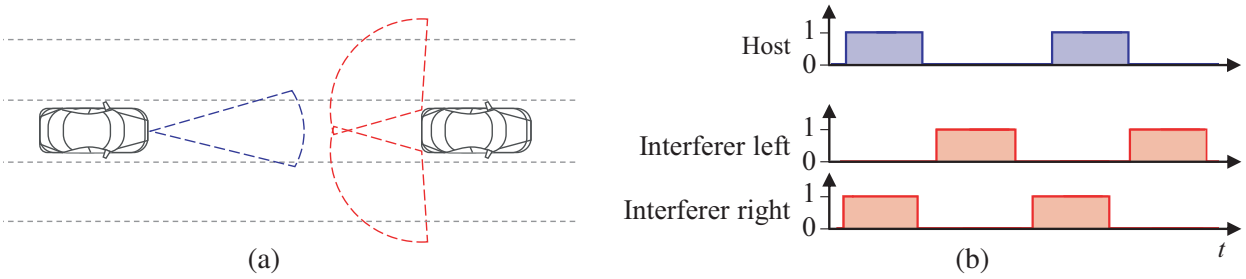

Figure 1. (a) Common multi-interferer scenario: The front mounted radar of the lift car might be interfered by the radars for blind spot monitoring of the right car due to an overlap of the fields of view. (b) Transmission cycles of the radars. The potential of interference from the right interferer is high in this example, while there is none form the left due to the overlap of the measurements in time.

on the radio channel. Varying numbers, positions and orientations of radar sensors result in various interference power levels at the host radar. Further statistical analysis of interference focusing on varying transmission frequencies has been presented in [10]. In contrast, in this paper, spatial conditions of the scenarios remain unchanged while the timing of the transmission of the radar sensors is randomized. Simple models for statistical interference evaluation have been presented in [11, 12] based on the work in [13].

In this publication, a method is introduced that combines the results of multiple single-interferer scenarios in order to simulate the reduction of the detection range due to interference in scenarios with multiple interferers.

2. DEGRADATION OF SNR AND DETECTION PERFORMANCE IN INTERFERED ENVIRONMENTS

The non-statistical model presented in this section underlies the model for statistical evaluation of interference introduced later in Section 3. The non-statistical model estimates the interference power I for a pair of FMCW radar sensors (interferer and host) with known sensor characteristics in a given scenario, considering line-of-sight interference only.

I and the resulting reduction of the detection range depend on the sensor characteristics of the interferer and the host as well as on the spatial and temporal circumstances given by the scenario. The principle signal flow of the model including input and output is shown in Fig. 2. The signal-to-interference ratio SIR according to [14] is given by

$$SIR = \frac{S}{N + C + I}. \tag{1}$$

where S is the signal power and C the clutter. The intrinsic system noise is given by

$$N = \sigma_N^2 T_{meas} f_{sample} G_{win}. \tag{2}$$

σ_N is the root mean square of the noise amplitude. Noise integrates incoherently, and thus linearly, over the total measurement period T_{meas} of all channels. f_{sample} is the sample frequency of the analog digital converter of the host, and G_{win} is the coherent integration gain of the applied window functions as shown in [15].

$C \ll I$ is assumed in the given scenarios to keep complexity manageable. The degradation of the SNR due to interference L_I can be calculated by

$$L_I = 1 + \frac{I}{N}. \tag{3}$$

The maximum detection range of non-interfered radar systems R_{det} is derived from the radar range equation [14]:

$$R_{det} = \left(\frac{P_{tx,H} G_{tx,H}(\theta_t) G_{rx,H}(\theta_t) RCS (T_{meas} f_{sample})^2 G_{win} \lambda^2}{(4\pi)^3 L_{int,H}^2 L_{rx,H} L_{tx,H} N SNR_{\min}} \right)^{0.25}. \tag{4}$$

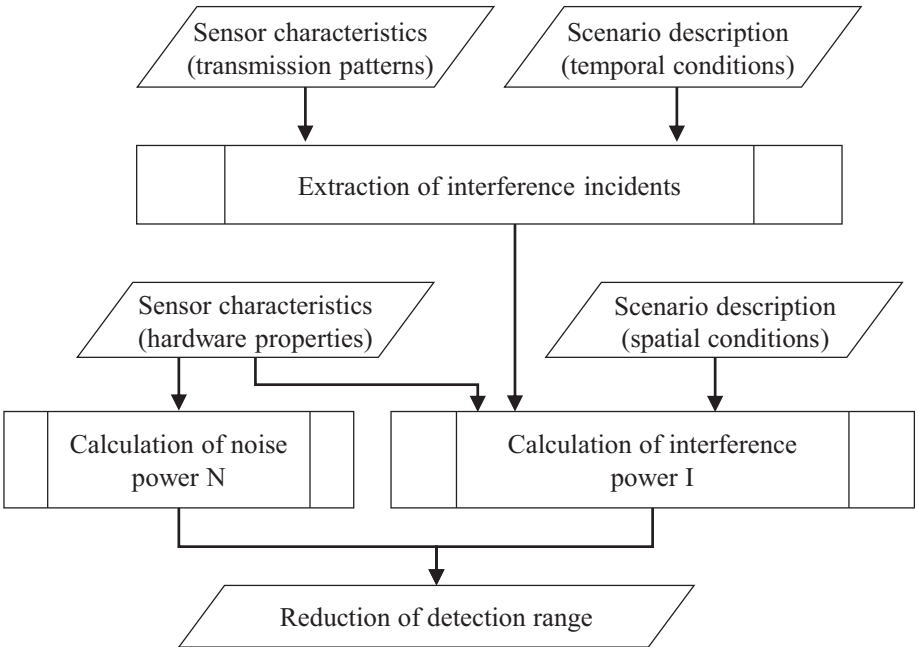

Figure 2. Signal flow of the basic non-statistical model underlying the statistic model.

The subscripted character H after a comma in a variable symbol indicates that the radar-specific variable relates to the host, while a subscripted I indicates a relation to the interferer. P_{tx} is the isotrope transmission power, G_{tx} the antenna gain of the transmitter, and G_{rx} the antenna gain of the receiver. RCS is the radar cross section of a target, and $SNR_{\min}$ is the adaptive detection threshold. L_{int} is the one-way integration loss while L_{rx} the power loss inflicted by the feeding lines from the receiver antenna to the MMIC. λ is the wavelength of the carrier frequency. If interference is considered, L_I is inserted into the denominator of the radicand of Eq. (4). The proportionate reduction of detection range L_R consequently can be calculated as

$$L_R = \frac{R_{det} - R_{det} L_I^{-0.25}}{R_{det}} = 1 - L_I^{-0.25}. \tag{5}$$

L_R is a well-suited qualifier for interference. It is graphic, and its dynamic is significantly lower than the dynamic of I or L_I. Further, it is independent from any target's radar cross section, from the applied detection threshold, and from the transmitting side of the host. Other effects of interference such as incidental ghost targets or decreased precision of the estimated velocity and direction of arrival of targets are not discussed, since they are minor for automotive applications.

2.1. Interference Power Estimation for Single Channels

The intersection of a single interferer-chirp with a single host-chirp is the core of the interference-power-model in this paper. Fig. 3 shows examples of three such interference incidents. All parameters belonging to one specific interference incident share the same index k. Since automotive radars often have multiple transmitters using time-domain multiplexing (TDM) or frequency-domain multiplexing (FDM) for larger virtual apertures, each interference incident usually does not affect all host channels at the same time but affects only a group of channels assigned to one host transmitter m. In order to estimate the interference power I_k of an individual interference incident, its duration $T_{I,k}$, its starting time t_{start}, k in relation to the host-chirp, its end time $t_{end,k}$, as well as the number i_k of the host-chirp in which the incident appeared must be known.

These parameters as well as the affected group of channels m are extracted using a geometric model based on [11]: The host-chirps are represented by vectors forming parallelograms in the time-frequency domain. The interferer-chirps are represented by lines as depicted in Fig. 3. By analyzing the positions

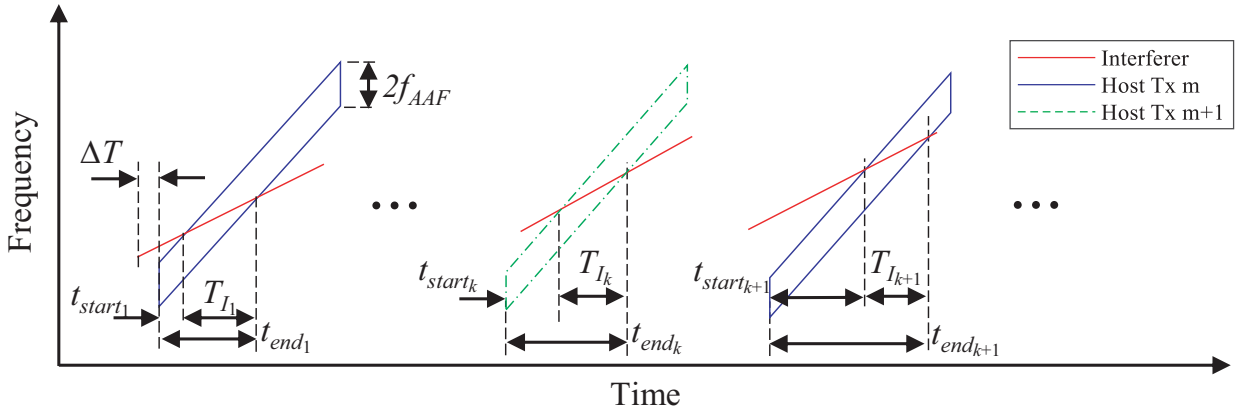

Figure 3. Visualization and geometric model of interference caused by the intersection of chirps of multi-chirp radars. The parallelograms represent the bandwidth of the intermediate frequency of the host radar, positioned around its transmitted chirps (blue: host transmitter m; green: host transmitter $m+1$). The red lines represent the interferer chirps.

of their intersections $t_{start,k}$, $T_{I,k}$, $t_{end,k}$, i_k, and m are extracted. Obviously, the time offset between the interferer measurement and the host measurement ΔT has a major effect on both the number of interference incidents and on their individual attributes. The interference power of each interference incident is given by

$$I = \frac{P_{I,EIRP} G_{win,k} G_{AAF,k} T_{I,k} f_{sample,H}}{L_{int,I} L_{int,H} L_{tx,I} L_{rx,H}}. \tag{6}$$

The calculation of the window gain $G_{win,k}$ requires the values of $t_{start,k}$, $t_{end,k}$, and i_k as input. The anti-aliasing filter gain $G_{AAF,k}$ is a function of $t_{I,k}$ [12]. The effective isotropic radiated power $P_{I,EIRP}$ of the interference source received by the host is determined using the one-way radar range equation as depicted in [13]:

$$P_{I,EIRP} = \frac{P_{tx,I} G_{tx,I}(\theta_H) G_{rx,H}(\theta_I) \lambda^2}{(4\pi)^2 R_I^2}. \tag{7}$$

$$P_{I,rx} = \frac{P_{tx,I} G_{tx,I}(\theta_H) G_{rx,H}(\theta_I) \lambda^2}{(4\pi)^2 L_{int,I} L_{int,H} L_{rx,H} R_I^2}. \tag{8}$$

The distance between the interferer and the host R_I is given by the scenario description. With the large number of chirps transmitted by automotive radars, multiple interference incidents are likely to appear in each measurement cycle. The interference power for each group of channels is estimated by summing up the interference power of all interference incidents in these channels [12].

$$I_m = \sum_{k=1}^{n_I} I_k, m. \tag{9}$$

2.2. Interference Power in Digital Beamforming Radars

The basic effect of digital beamforming (DBF) on interfered radar measurements was investigated in [16] and [17]. This section describes how to model the angular dependent proportion of I in DBF radars, using the signal model depicted in [18] and [19]. If the host is a single-input multiple-output radar, the interference signal of each of the n_{rx} receiver channels with the index n is defined as

$$X_{I,n} = \sqrt{I} \exp\left(\frac{2\pi j}{\lambda} p_{rx,n} \sin\theta_I\right) \tag{10}$$

where j is an imaginary number, θ_I the direction of the interference source in relation to the host, and $p_{rx,n}$ the position of the receiver antenna relative to the transmitter antenna. I has the same amplitude

in each channel. The phase difference between the channels depends on λ, θ_I, and $p_{rx,n}$. If the host is a TDM or FDM multiple-input multiple-output (MIMO) radar with n_{tx} transmitters, each group of virtual channels assigned to one transmitter is interfered individually. Therefore, $\vec{I}$ is an n_{tx}-element vector with the elements I_m. The interference signal of each virtual channel is defined as

$$X_{I,m,n} = \sqrt{I_m} \exp\left(\frac{2\pi j}{\lambda}(p_{tx,m} + p_{rx,n}) \sin\theta_I + j\varphi_m\right). \tag{11}$$

φ_m is the additional random phase of each group of virtual channels assigned to the transmitter m. If stacked into one single column vector $\vec{X}_I$, the entirety of interference signals is given by

$$\vec{X}_I = \left(\sqrt{\vec{I}} \otimes \vec{1}_{rx}\right) \circ \exp\left(\frac{2\pi j}{\lambda}(\vec{p}_{tx} \otimes \vec{1}_{rx} + \vec{1}_{tx} \otimes \vec{p}_{rx}) \sin\theta_I + j\vec{\varphi} \otimes \vec{1}_{rx}\right) \tag{12}$$

where $\otimes$ is the Kronecker product, $\vec{1}_{n,rx}$ the column vector of ones with n_{rx} elements, and $\circ$ the Hadamard product. Since only the phase difference between the channels is important for digital beamforming instead of the absolute phase values, the size of the vector $\vec{\varphi}$ is reduced by one dimension for faster simulation in Section 4:

$$\Delta\vec{\varphi} = \left(\varphi_2 - \varphi_1, \varphi_3 - \varphi_1, \ldots, \varphi_{n,tx} - \varphi_1\right)^T. \tag{13}$$

The conventional beamformer is the applied beamforming technique [20], so the interference power I_θ in a direction θ is given by:

$$I_\theta = \vec{v}_I(\theta)^T R_{X,I} \vec{v}_I(\theta) \tag{14}$$

where $R_{X,I}$ is the estimated covariance matrix of $\vec{X}_I$, and $\vec{v}_I$ is the weighting vector consisting of the expected signals for each channel for a given angle θ

$$\vec{v}_I(\theta) = \exp\left(\frac{2\pi j}{\lambda}\left(\vec{p}_{tx} \otimes \vec{1}_{n,rx} + \vec{1}_{n,tx} \otimes \vec{p}_{rx}\right) \sin\theta\right) \tag{15}$$

3. STATISTICAL ANALYSIS OF SNR AND RANGE REDUCTION

Artificial interference varies largely, so statistical analysis is mandatory. For particular sensor setups and scenarios, I_θ can be calculated with the model described in Section 2, using specific values for ΔT and $\Delta\vec{\varphi}$. However, the parameters ΔT and $\Delta\varphi$, which have a major effect on I_θ, are significantly statistically distributed. Therefore, they are considered random variables in the presented model.

3.1. ΔT Dependency

As stated in Section 2.1, ΔT has a major influence on the interference power I. If there is no time synchronization between interferer and host, ΔT can be considered uniformly distributed.

$$f_{\Delta T}(x) = \mathrm{unif}\big(0, \min\left(T_{cycle,I}, T_{cycle,H}\right)\big) \tag{16}$$

where $T_{cycle,I}$ is the duration of the measurement cycles of the interferer, and $T_{cycle,H}$ relates to the host. Corresponding to Eqs. (6) and (8), I_m takes different values for different interference incidents, hence for each ΔT. The distribution function of the random variable I_m is described as

$$f_{I,m}(x) = P(I_m = x), x \in \mathbb{R}^{\geq 0}. \tag{17}$$

3.2. $\Delta\vec{\varphi}$ Dependency

As shown in Eqs. (10) and (11), the distribution of I_θ over the angular spectrum in DBF MIMO systems is, in addition to being determined by $f_{I,m}$, also determined by the multivariate random variable $\Delta\vec{\varphi}$. The value of each φ_m is considered uniformly distributed

$$f_{\varphi_m}(x) = \mathrm{unif}(0, 2\pi). \tag{18}$$

Further, the values of different φ_m are disjointed from each other and ΔT. With this given, I_θ is a random variable with the probability distribution function

$$f_{I,\theta}(x) = P(I_\theta = x), \quad x \in \mathbb{R}^{\geq 0} \tag{19}$$

with N being independent from ΔT and $\Delta\varphi$, Eq. (18) inserted into Eq. (5) results in the distribution functions of the random variable $f_{L_R,\theta}$

$$f_{L_R,\theta}(x) = P(L_R = x), x \in [0, 1[. \tag{20}$$

3.3. Statistics of Multiple Interferers

Source [21] states that two independent random variables X and Y can be summed together as $X + Y = Z$ by the convolution of their individual distributions, if they apply to

$$f_Z(x) = P(Z = x) = P(X + Y = x), \quad x \geq 0. \tag{21}$$

Assuming that $\sum_{T_{I,k}} \ll T_S$, clipping as a result of multiple simultaneous interference incidents is not considered relevant. Thus, $I_{\theta,1}$ and $I_{\theta,2}$ of different interferers targeting the same host qualify for summation by the convolution of their distribution functions

$$f_{I_{1+2},\theta} = f_{I_1,\theta} * f_{I_2,\theta}. \tag{22}$$

If more than two interferers are present, sequential convolutions of the allocated probability distributions are executed

$$f_{I,\theta} = f_{I_1,\theta} * f_{I_2,\theta} * \ldots * f_{I_{last},\theta}. \tag{23}$$

Convolution as in Eqs. (21) and (22) must not be applied analogously on $f_{L_R,\theta}$ since it does not follow the rule stated in Eq. (20). The reduction of the detection range as a result of multiple interferers is instead determined indirectly via $f_{I,\theta}$.

3.4. Simulation Approach

Since the model introduced in Section 2 consumes little computational power, it is feasible for iteration with altering inputs for ΔT and $\Delta\vec{\varphi}$ in a Monto Carlo method. The distributions of the random variables ΔT and $\Delta\vec{\varphi}$ are uniform, as described in Eqs. (15) and (17). In order to get representative results from the Monte Carlo method with fewer trials, ΔT and $\Delta\vec{\varphi}$ are consecutively changed within their range by the equally sized increments ΔT_{inc} and $\vec{\varphi}_{inc}$ in each simulation step (Fig. 4). These iterations are performed for each interferer with the index a, leading to a total of n_{sim} simulation steps:

$$n_{sim} = \frac{\min(T_{cycle,I}, Tcycle, H)}{T_{inc}} \left(\frac{2\pi}{\varphi_{inc}}\right)^{n_{tx}-1} n_I \tag{24}$$

where n_I is the total number of interferers. The computing time of the simulation grows roughly linearly with n_{sim}.

4. VALIDATION OF THE STATISTICAL MODEL

The setup for the validation of the statistical model is based on the scenario pictured in Fig. 1(a). It is specifically shown in Fig. 5(a): The device under test, the host, is placed centrally 10 m behind a vehicle that is equipped with two interfering short-range radars at the back. These are installed behind the bumper at a 45° angle. The device under test as well as the interfering vehicle remain still during the measurements. The hardware parameters and the transmission patterns of the involved radar sensors are listed in Table 1. The transmission pattern of the device under test is aligned with modulations of automotive FMCW-far-range radars. Four different sets of measurements are conducted, each consisting of 750 measurement cycles with individual interferers active:

- First, only the left interferer active,
- Second, only the right interferer active,
- Third, both interferers active, and

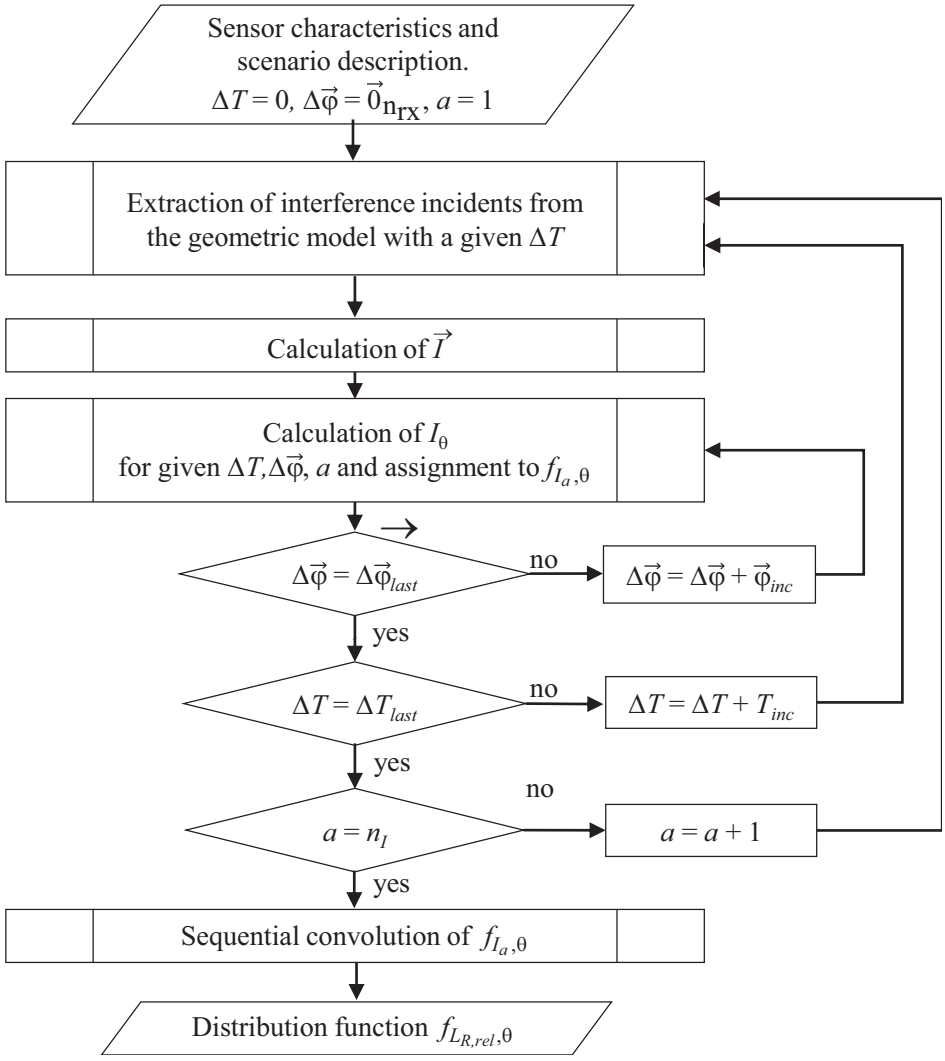

Figure 4. Flowchart of the statistical simulation. The two inner loops calculate the distribution of I for each interferer. These distributions are convoluted afterwards to receive the interference statistics of multi-interferer scenarios. ΔT_{last} and $\Delta\vec{\varphi}_{last}$ refer to the maximum values as shown in Eqs. (15) and (17).

- Fourth, both interferers switched off as reference.

Two exemplary measurements taken form the third and forth sets of validation measurements are shown in Fig. 5(b). An ordered-statistics constant false alarm rate detector is applied to generate a dynamic threshold. The diagram shows that the small detections numbered as 2.4 and 5 are lost due to the increased noise floor. The angle-dependent arithmetic mean of the reduction of the detection range over all measurements cycles, range and velocity gates in respect to the reference measurements is calculated and compared with simulation results in Fig. 6. The simulation parameters are set to $\Delta T_{inc} = 400\,\mu s$ and $\varphi_{inc} = 36°$, resulting in 1000 simulations or each interferer in each scenario.

The significant difference between the amplitudes of the first and second measurement sets can be attributed to tolerances regarding the bumper thickness and the transmission power of the short-range radars. These tolerances lead to deviations from the assumed $P_{I,EIRP} \cdot L_{int}$ of several dB. In the third measurement set, these deviations lead to a slight shift of the peak-average interference direction toward the stronger interferer on the right-hand side. Further, Fig. 7 shows the probability distributions of the reduction of the detection range at 0° with both interferers active.

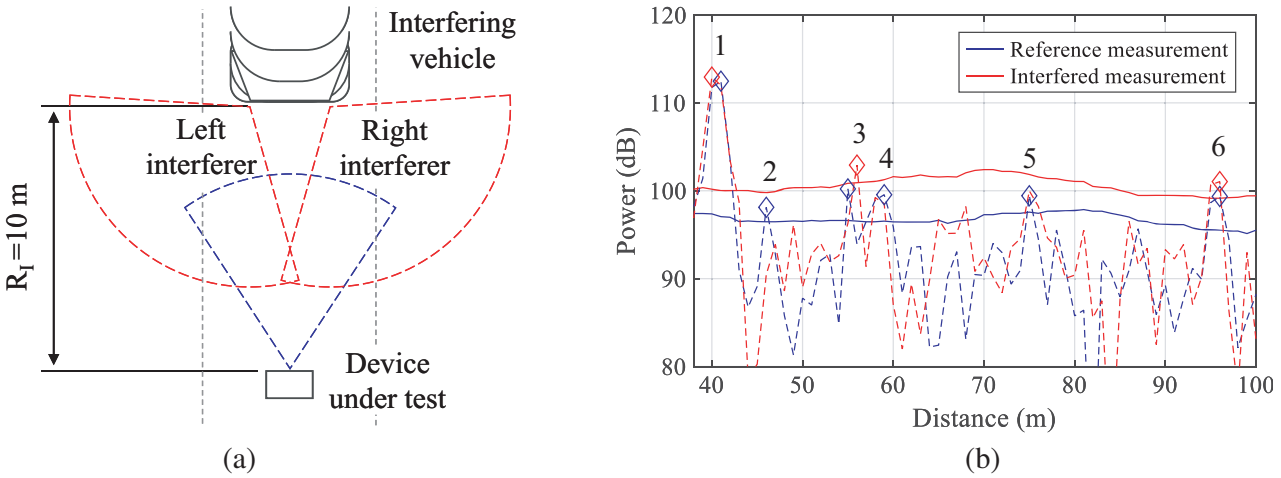

Figure 5. (a) Setup for validation measurements. (b) Range-Spectra at $\theta = 0°$ and velocity $= 0\,\mathrm{m/s}$ taken from the third and the fourth set of validation measurements. Dotted lines represent the raw spectrum, full lines represent the detection threshold, diamond markers the detections.

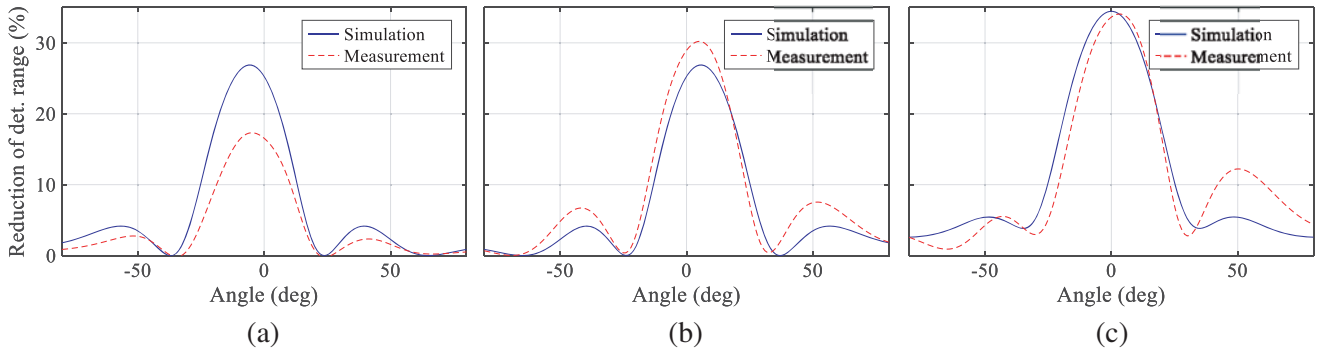

Figure 6. Comparison of the simulated and the measured mean reduction of the detection range in different interferer setups. (a) Left interferer active. (b) Right interferer active. (c) Both interferers active.

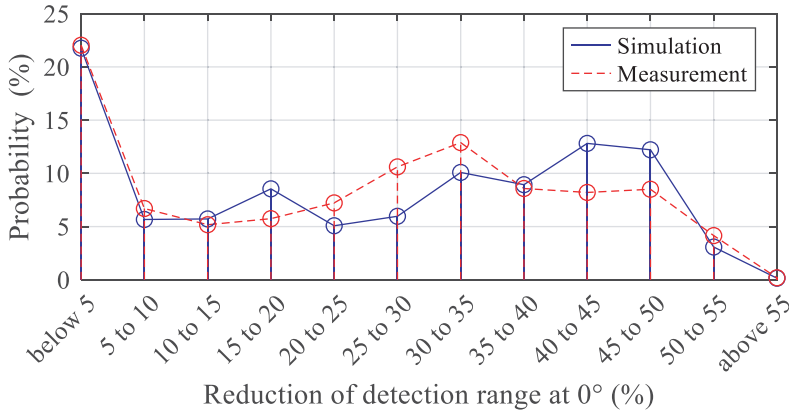

Figure 7. Comparison of the simulated and the measured mean reduction of the detection range in the direction of 0° when both interferers are active. Distribution of 1000 sample simulation runs and 750 sample measurement cycles.

Table 1. Sensor characteristics: Values of the host used for the validation measurements that differ from the settings used for the simulations in Section 5 are bracketed.

Symbol	Quantity	Values, interferering radar	Values, host radar
$\vec{p}_{tx}$	Positon tx antennas	-	$1.9 \cdot [0\ 1\ 2\ 3]$ mm
$\vec{p}_{rx}$	Positon rx antennas	-	$1.9 \cdot [0\ 4]$ mm
P_{tx}	Isotrope transmission power	10 dBm	-
$G_{tx}(0°)$	Tx antenna gain at 0°	13.5 dB	-
$G_{tx}(5°)$	Tx antenna gain at 5°	10.5 dB	-
$G_{rx}(0°)$	Rx antenna gain at 0°	-	16 ($\sim$ 10) dB
$G_{rx}(50°)$	Rx antenna gain at 50°	-	15.3 ($\sim$ 9.5) dB
L_{rx}	Receiver loss	-	4 dB
L_{tx}	Transmitter loss	4 dB	-
L_{int}	One way integration loss	2 dB	2 dB
σ_N	RMS noise	-	-87.88 dBm
f_{sample}	Sample frequency	-	10 MHz
f_{AAF}	Frequency of AAF of intermediate frequency	-	8 MHz
-	Mid. frequency	76.5 GHz	76.5 GHz
λ	Mid. wavelength	-	3.9 mm
-	Chirp bandwidth	950 MHz	100 MHz
-	Total chirps per channel	256	256 each tx
T_{chirp}	Duration of each chirp	45 µs	25.6 µs
-	Chirp repetition rate	50 µs	30 µs
T_{cycle}	Cycle time	40 ms	75 ms

5. SIMULATION OF RANGE REDUCTION IN A HIGHWAY SCENARIO WITH MULTIPLE INTERFERERS

The consequences of reduced detection ranges are particularly negative in highway scenarios, in which the ego vehicle and other road users travel at high velocities. In addition, numerous radars might be interfering at the same time on multilane roads. Therefore, the reduction in the detection range of a front-mounted far-range radar in a highway scenario depending on different quantities of interferers is simulated in this section.

5.1. Scenario and Sensor Setup Definition

The layout of the given scenarios is pictured in Fig. 8. It contains a host vehicle in the middle lane of a multilane highway and interfering vehicles in the neighboring lanes as well as a single vehicle in the same lane. The interfering vehicles and the host vehicle share their installation configuration with the setup described in Section 4 and Fig. 1. However, if interfering vehicles are positioned in a neighboring lane, only the radars on the "host-side" of the interfering vehicles are taken into account. This is because of the low transmission powers of the selected corner radars at angles greater than 45°.

In five defined scenarios, labeled 1 to 5, different interferers are active (Table 2). The sensor characteristics used in the simulation are shown in Table 1. Scenarios 1 to 3 provide information about the reduction of the detection range as a result of a gradually increasing number of interferers in only one neighboring lane. Scenario 4 shows the effect of multiple interfering radars in both neighboring tracks. Scenario 5 includes active interferers in all lanes.

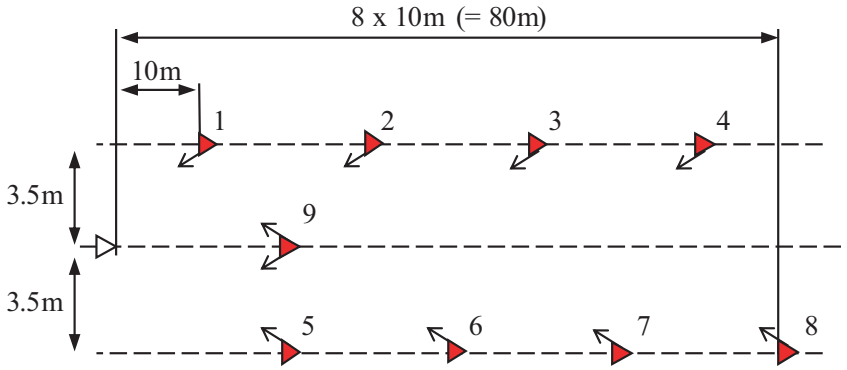

Figure 8. The white triangle represents the host vehicle and the red triangles represent vehicles with interfering radars whose boresight directions are pictured as black arrows.

Table 2. Interferer configurations for the simulated scenarios. Indices in the second column refer to Fig. 8.

Scenario name	Indices of interfering vehicles with activated radars
1	1
2	1, 2
3	1, 2, 3, 4
4	1, 2, 3, 4, 5, 6, 7, 8
5	1, 2, 3, 4, 5, 6, 7, 8, 9

5.2. Simulation Results

The simulation parameters are the same as those in Section 4. Fig. 9 shows the expected mean range loss over the angular spectrum for the simulated scenarios. Fig. 10 shows the probability distributions of the reduction of the detection range at 0°.

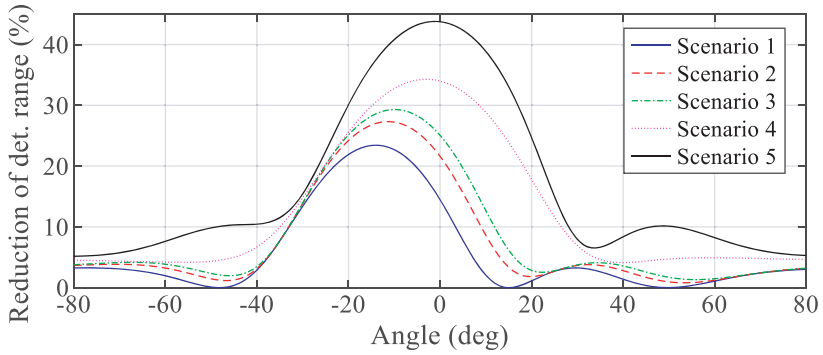

Figure 9. Simulation of the mean reduction of detection range in different scenarios for different directions.

The comparison of scenarios 1, 2, and 3 shows that with growing numbers of interferers in one neighboring lane, the detection range is reducing. However, the additional reduction decreases with each added interferer. This can be attributed to two main factors: Firstly, $P_{I,EIRP}$ decreases quadratically with the distance between the interferer and the host as shown in Eq. (7). Due to the limited space in the immediate surroundings of the host, the distance to additional interfering vehicles grows in the

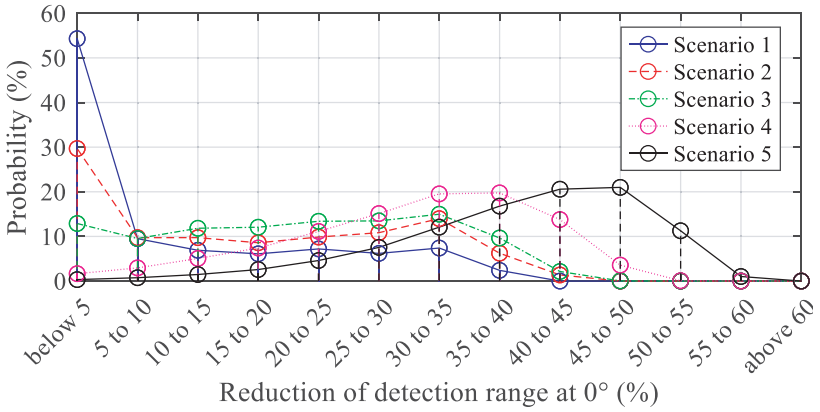

Figure 10. Simulation of the probability distribution of the reduction of detection range in the direction of 0°.

given scenario layout and thus $P_{I,EIRP}$. Secondly, according to Eq. (5), the detection range decreases only with the fourth root of the interference power, which for its part grows linearly with the number of interferers. The Beamformer focuses I_θ in the direction of the interference source, so the impact of interferers in the neighboring lane on detections on the most relevant ego-lane seems manageable. The directivity of the antennas of the host turns out to be beneficial as well. From a functional standpoint, scenario 4 has been proven to be the worst-case scenario examined in this paper: Numerous interferers in both neighboring lanes lead to a great reduction of the detection range in the ego-lane, while there are no preceding vehicles in the lane with relatively large radar cross sections reacting to small targets like debris. Therefore, the host vehicle cannot align its actions to a car ahead. Moreover, in less than 2% of all simulations the range reduction is below 5%, so noticeable performance degradation is observed in the great majority of cases.

As expected, the heaviest interference can be found in scenario 5, in which interferers are in the immediate surroundings of the host in all lanes. The average reduction of detection range at 0° is 43.7% with more than 50% of the measurements cycles having their range reduced to less than 60%. However, since all lanes in front of the host are blocked, its automated driving behavior will be aligned largely with the surrounding cars: Long detection ranges are of lesser importance in this scenario.

6. CONCLUSION

The introduced model can be used for the statistical analysis of the detection performance of automotive radars during the presence of interference by multiple radars. Complimentary measurements have proven the model sufficiently correct to provide significant information about the reduction of the detection range in multi-interferer scenarios. Sample simulations of multi-interferer environments show that in the case of high market penetration rates of radars, even an average reduction of the detection range of more than 30% is possible on crowded highways. The chance of measurement cycles that are not interfered or only negligibly so is reduced to a minimum if numerous interferers are present. However, a reduction of the detection range above 55% is unlikely to appear even in heavily interfered environments. This is due to the limited space for interfering vehicles in the immediate surroundings in the line of sight of the host and because of the degressive proportionality of range loss to interference power.

Still, the outlined interference-caused reduction of detection range has significant effects on the functions of automotive radars. Therefore, without harmonization and sophisticated repairing of interfered signals, a detection range reserve will be inevitable for future automotive radars with increasing market penetration.

REFERENCES

1. Winner, H., S. Hakuli, F. Lotz, and C. Singer, *Sensors for DAS*, Springer, Switzerland, 2016.

2. Oprisan, D. and H. Rohling, "Analysis of mutual interference between automotive radar systems," *International Radar Symposium (IRS)*, 83–90, Berlin, Germany, 2005.
3. Brooker, G. M., "Mutual interference of millimeter-wave radar systems," *IEEE Trans. Electromagn. Compat.*, Vol. 49, No. 1, 170–181, 2007.
4. Goppelt, M. and H.-L. Blöcher, "Automotive radar — Investigation of mutual interference mechanisms," *Advances in Radio Science*, Vol. 8, 55–60, 2010.
5. Schipper, T., et al., "Simulative prediction of the interference potential between radars in common road scenarios," *IEEE Trans. Electromagn. Compat.*, Vol. 57, No. 3, 322–328, 2015.
6. Schipper, T., et al., "A simulator for multi-user automotive radar scenarios," *IEEE MTT-S Int. Conf. Microwaves Intell. Mobility*, 1–4, 2015.
7. Al-Hourani, A., R. J. Evans, S. Kandeepan, B. Moran, and H. Eltom, "Stochastic geometry methods for modeling automotive radar interference," *IEEE Transactions on Intelligent Transportation Systems*, Vol. 19, No. 2, 333–344, 2017.
8. Munari, A., L. Simić, and M. Petrova, "Stochastic geometry interference analysis of radar network performance," *IEEE Communications Letters*, Vol. 22, No. 11, 2362–2365, 2018.
9. Terbas, D., F. Laghezza, F. Jansen, A. Filippi, and J. Overdevest, "Radar to radar interference in common traffic scenarios," *16th European Radar Conference (EuRAD)*, 177–180, 2019.
10. Skaria, S., A. Al-Hourani, R. J. Evans, K. Sithamparanathan, and U. Parampalli, "Interference mitigation in automotive radars using pseudo-random cyclic orthogonal sequences," *Sensors*, Vol. 19, 4459, 2019.
11. Hahmann, K., S. Schneider, and T. Zwick, "Evaluation of probability of interference-related ghost targets in automotive radars," *2018 IEEE MTT-S International Conference on Microwaves for Intelligent Mobility (ICMIM)*, 1–4, 2018.
12. Hahmann, K., S. Schneider, and T. Zwick, "Estimation of the influence of incoherent interference on the detection of small obstacles with a DBF radar," *2019 IEEE MTT-S International Conference on Microwaves for Intelligent Mobility (ICMIM)*, 1–4, 2019.
13. Schipper, T., "Modellbasierte analyse des interferenzverhaltens von Kfz-Radaren," Ph.D. dissertation, Karlsruhe Instituite of Technology, 2017.
14. Richards, M., J. Scheer, and W. Holm, "The radar range equation," *Principles of Modern Radar*, SciTech, Raleigh, NY, 2010.
15. Harris, F. J., "On the use of windows for harmonic analysis with the discrete Fourier transform," *Proceedings of the IEEE*, Vol. 66, No. 1, 51–83, 1978.
16. Fischer, C., H.-L. Blöcher, J. Dickmann, and W. Menzel, "Robust detection and mitigation of mutual interference in automotive radar," *2015 16th International Radar Symposium (IRS)*, 143–148, 2015.
17. Fischer, C., M. Goppelt, H.-L. Blöcher, and J. Dickmann, "Minimizing interference in automotive radar using digital beamforming," *Advances in Radio Science*, Vol. 9, 45–49, 2011.
18. Bechter, J., K. Eid, F. Roos, and C. Waldschmidt, "Digital beamforming to mitigate automotive radar interference," *2019 IEEE MTT-S International Conference on Microwaves for Intelligent Mobility (ICMIM)*, 1–4, 2016.
19. Bechter, J., M. Rameez, and C. Waldschmidt, "Analytical and experimental investigations on mitigation of interference in a DBF MIMO Radar," *IEEE Transactions on Microwave Theory and Techniques*, Vol. 65, No. 5, 1727–1734, 2017.
20. Bartlett, M., "Smoothing periodograms from time-series with continuous spectra," *Nature*, Vol. 161, 686–687, 1948.
21. Bosq, D. and H. T. Nguyen, "Basic probability background," *A Course in Stochastic Processes*, Springer, Dordrecht, 1996.